Assessing sponge cities performance at city scale using remotely sensed LULC changes
Case study Nanjing

Liu, Xiaolong; Fu, Dafang; Zevenbergen, Chris; Busker, Tim; Yu, Meixiu

Important note
To cite this publication, please use the final published version (if applicable).
Please check the document version above.

Article

Assessing Sponge Cities Performance at City Scale Using Remotely Sensed LULC Changes: Case Study Nanjing

Xiaolong Liu [1,2,3,*], Dafang Fu [1], Chris Zevenbergen [2,3], Tim Busker [4] and Meixiu Yu [5]

1   School of Civil Engineering, Southeast University, Nanjing 211189, China; fdf@seu.edu.cn
2   IHE Delft Institute for Water Education, 2611AX Delft, The Netherlands; c.zevenbergen@un-ihe.org
3   Faculty of Civil Engineering and Geosciences, Delft University of Technology, 2628CN Delft, The Netherlands
4   Institute for Environmental Studies (IVM), Vrije Universiteit Amsterdam (VU),
    1081HV Amsterdam, The Netherlands; tim.busker@vu.nl
5   College of Hydrology and Water Resources, Hohai University, Nanjing 210098, China; meixiuyu@hhu.edu.cn
*   Correspondence: 230179096@seu.edu.cn

Abstract: As a result of high-density urbanization and climate change, both the frequency and intensity of extreme urban rainfall are increasing. Drainage systems are not designed to cope with this increase, and as a result, floods are becoming more common in cities, particularly in the rapidly growing cities of China. To better cope with more frequent and severe urban flooding and to improve the water quality of stormwater runoff, the Chinese government launched the national Sponge City Construction (SCC) program in 2014. The current SCC design standards and guidelines are based on static values (e.g., return periods, rainfall intensities, and volume capture ratio (VCR)). They do not fully acknowledge the large differences in climate conditions across the country and assume that the hydraulic conditions will not change over time. This stationary approach stems from the traditional engineering approach designed for grey infrastructure (following a "one size fits all" approach). The purpose of this study was to develop a methodology to assess the VCR baseline (before construction in the pre-development stage) and changes in VCR (difference between the VCR of the pre- and post-development stage). The VCR of the post-development stage is one of the required indicators of the Assessment Standard for Sponge Cities Effects to evaluate SCC projects. In this study, the VCR was derived from remote-sensing-based land use land cover (LULC) change analysis, applying an unsupervised classification algorithm on different Landsat images from 1985 to 2015. A visualization method (based upon Sankey chart, which depicts the flows and their proportions of components) and a novel and practical partitioning method for built-up regions were developed to visualize and quantify the states and change flows of LULC. On the basis of these findings, we proposed a new indicator, referred to as $VCRa - L$, in order to assess the changes in urban hydrology after SCC construction. This study employed the city of Nanjing as a case study and analyzed detailed information on how LULC changes over time of built-up areas. The surface area of the urban and built-up areas of Nanjing quadrupled from 11% in 1985 to 44% in 2015. In the same period, neither the entire city nor its subregions reached the VCR target of 80%. The proposed new methodology aims to support national, regional, and city governments to identify and prioritize where to invest and implement SCC measures more effectively in cities across China.

Keywords: sponge city construction; volume capture ratio; land use change; remote sensing; modified Sankey chart; built-up area partitioning method; Google Earth Engine

1. Introduction

With the implementation of the economic reform policy in 1978, the gross domestic product (GDP) of China has experienced an explosive increase along with urban expansion, especially in the eastern provinces. This rapid urban development has attracted a large number of the non-urban population, leading to massive urban migration. In turn, this has resulted in severe environmental damage, affecting human health and wellbeing of the

Chinese urban population. The total amount of pollutants emitted by domestic and commercial activities, transportation, and industrial production has increased exponentially, exceeding the regional environmental carrying capacity [1–5]. A significant fraction of the emitted pollutants is transported with rainfall and runoff, having a severe chemical and ecological impact on the status of urban surface water bodies [3–6]. Moreover, urbanization leads to an increase of impervious area, which intensifies the hydrological cycle and increases the occurrences of extreme events such as droughts and floods [7–9].

Various concepts and solutions have been identified and implemented over the world, in order to reduce urban water pollution and to mitigate the adverse impacts of too much and/or too little rainfall, both in developed and developing countries. Some of them aim to expand the capacity of conventional gray infrastructure drainage systems, by using leaping weirs to intercept initial runoff, or by the construction of an underground storage facility to store large volumes of stormwater [10,11]. Green infrastructure is increasingly used to mitigate the impact of urban stormwater on both the quantity and quality of urban runoff. Approaches and strategies using green infrastructure to manage urban stormwater are referred to as best management practices (BMPs) in the United States and Canada [12,13], water-sensitive urban design (WSUD) in Australia and New Zealand [14], sustainable urban drainage systems (SuDS) in the United Kingdom and other EU countries [15–17], the Active Beautiful Clean Waters plan (ABC Water) in Singapore [18], and the Sponge City Construction (SCC) in China [19,20].

In terms of the design and assessment of Sponge City infrastructure, the *volume capture ratio of annual rainfall* (VCRa) is one of the compulsory indicators of the national SCC standard launched by the Ministry of Housing and Urban–Rural Development (MOHURD) in 2014 [20,21]. Examples of its application encompass Sponge City infrastructure projects covering an area ranging from a few to several hundred hectares [22]. The VCRa target value varies across China and is dependent on geographical factors such as climate, soil, and vegetation cover. Currently, a methodology is lacking to assess the spatial variation of VCRa at a city scale and changes therein over time, which hampers city planners to prioritize and select SCC interventions to comply with the SCC targets. This paper aims to present a method, based on land use and land cover (LULC) data derived from satellite remotely sensed images, to set a baseline of VCRa on city and district level required to identify, prioritize, design, and evaluate SCC projects by taking into account the VCRa in their pre-development stage.

2. Volume Capture Ratio of Annual Rainfall (VCRa)

The volume capture ratio of annual rainfall (VCRa) is defined as the fraction (expressed as a percentage) of the total annual rainfall that is not directly discharged (the cumulative annual control) but detained or retained by means of natural and artificial enhancement such as infiltration, storage, and evaporation [20].

The VCRa is a regional variant for calculating the water quality volume (WQv) in China [21]. Comparably, another similar practice by capturing the 85th to 95th percentile rainfall event has also been widely used [23–27]. The VCRa is based on the total captured stormwater volume of the survey site and does not consider the frequency of storm events [20,21,28]. Previous studies of VCRa mainly focused on three aspects: (i) regional application, (ii) case design application, and (iii) efficiency assessment of SCC measures or low impacted development (LID). With regards to its *regional application*, a map of China divided into regions with similar VCRa values was adopted in the SCC guide of the Ministry of Housing and Urban–Rural Development [20,29]. Li et al. [29] and Zhang et al. [21] proposed a design rainfall map corresponding to VCRa of 85% for the mainland of China. Although both maps are recommended for general application covering the whole country, the dataset used contains 186 rainfall stations [29,30], which is likely too limited to cover the more than 600 cities in China. Site-specific urban stormwater and flood models are commonly used methods for site design and assessment of VCRa. Liu et al. [31] developed an urban flood model (HIMS-URBAN) for the central area of Changde to design

a Sponge City infrastructure project based on a short-duration design rainfall profile. Wang et al. [32] conducted a similar simulation using the Storm Water Management Model (SWMM) with gauged rainfall covering a period of three consecutive years. In both studies, a short-duration composite runoff coefficient was calculated to design the SCC project [31,32]. Randall et al. simulated four hypothetical scenarios including No LID (baseline), Low LID, Mid LID, and High LID measures for an urban catchment of 133 km^2 in Beijing to evaluate the feasibility of the VCRa target using SWMM [22]. Long-term (more than 30 years) continuous simulations were conducted on the basis of the conditions of the current landscape and stormwater infrastructure. On the basis of this study, the authors concluded that the computed VCRa served as a meaningful indicator to compare the effectiveness of the scenarios before and after the installation of SCC measures. In terms of efficiency assessment of SCC/LID measures, there is a wealth of publications focusing on the performance of LID measures and their design to meet water quantity and quality goals, such as from Hunt et al. [33–35], Cizek et al. [36], Braga et al. [37], and Drake et al. [38,39].

Various design manuals of SCC have been issued by the Chinese central government, and design targets have been set for different cities or regions [20,40]. For example, the VCRa of Nanjing for 2030 has been targeted at 80% [41,42]. A short-duration composite runoff coefficient is predominantly being used to assess the VCRa baseline on project site-level or district level [31,32,43], and the captured volume estimate is based upon urban stormwater management models [22,44]. Although methods to assess a short-duration composite runoff coefficient can be applied at the city level, a direct comparison with the design target of the VCRa is constrained due to the fact that the accuracy and precision of the underlying computer modeling of these methods are contested. This is partly due to the increasing complexity of urban stormwater simulation and the incompleteness or lack of high-resolution geospatial data affected by intense human activities [45]. The purpose of this study is to establish a method for a rapid global baseline assessment before the implementation of SCC measures.

3. Site Design

Nanjing, the capital city of Jiangsu province, is one of the megacities of the Yangtze River Delta Megalopolis in East China. Figure 1 depicts the study area with a radius of 20 km and a total surface area of 1256 km^2, which covers a major part of the city of Nanjing. With a rapid economic growth, the GDP and population of Nanjing reached USD 191.1 billion and 8.245 million inhabitants, respectively, by the end of 2018 [46]. While economic growth has improved the livelihoods of the inhabitants, it has also led to urban congestion and a reduced capacity to manage extreme natural disasters. Since 2016, various green infrastructure projects and SCC technologies have been implemented in Nanjing to compensate against the environmental impacts of urbanization. VCRa targets of over 80% for new-built or refurbishment projects and over 70% for built areas have been adopted by the Nanjing city government. In addition, ambitious goals of "*more than 20% of the built-up area have to comply with the requirements of the SCC targets by 2020*" and "*more than 80% will by 2030*" were established [41,42]. Due to a lack of background information, it is difficult to assess the feasibility of these goals, which greatly reduces its guidance role for the SCC practices and measures chosen. The method designed in this paper is aimed to improve upon this gap.
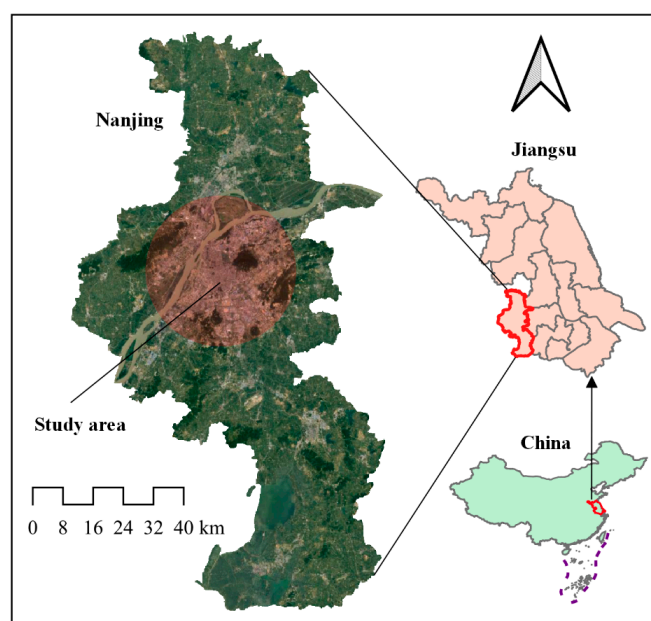
Figure 1. The study area of Nanjing, Jiangsu, China. Background from Google Earth Imagery [47].

Compared to regular administrative division, a simple but effective division method has been used in Nanjing, whose administrative boundaries change frequently due to the rapid development of the economy and urbanization [48]. Four concentric circles with an increasing 5km step radius were drawn to analyze the relationship between landscape changes and distance from the center to outskirt, taking the Bronze Statue of Sun Yat-sen in Xinjiekou as the centroid to forming four concentric zones (Figure 2). The surface area of the zones from the innermost to the outermost were 25π, 75π, 125π, and 175π square kilometers, respectively. From space, cities look like a kind of scratch on the planet surface, lacking uniformity or central symmetry. The concentric zones were divided by two cross-lines through the centroid in order to capture the orientation of urban expansion. These two lines were set east-westward and north-southward to separate the areas of the concentric pie zones into quarters. This partitioning of urban area can also be applied to analyze other cities with a top-down planning and frequently changing administrative boundaries.
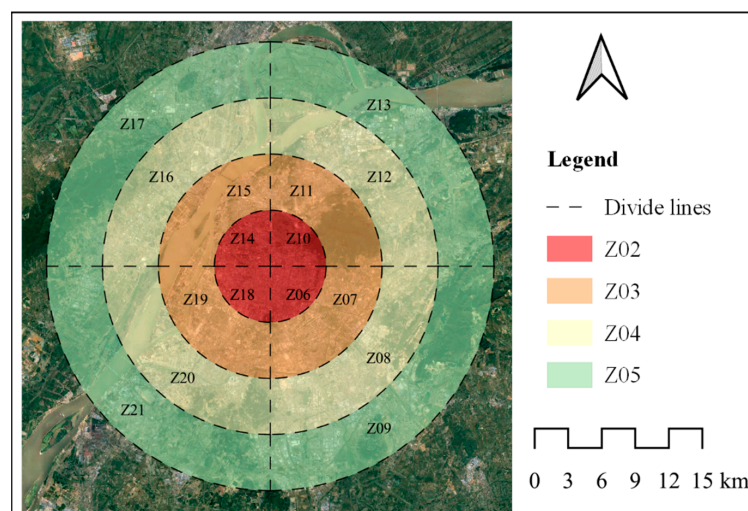

Figure 2. Partitioning of urban area as designed for Nanjing. The entire region was abbreviated as Z01, which covers the majority of the urban area. The concentric zones were distinguished with different colors (Z02–Z05). The concentric pie zones were annotated by text (Z06–Z21). Background from Google Earth Imagery [49]. The center was set at the Bronze Statue of Sun Yat-sen in Nanjing.

4. Data and Methods

4.1. Data and Classification

The Landsat program has the longest continuous space-based record of the Earth's surface in existence [50,51]. On the basis of the service time and operational status of the Landsat satellites, we chose a set of images to prepare the high-quality imagery for each year (Table 1) after the removal of the clouds and compositing operation. The Weka *k*-means clustering algorithm with 30 clusters was used to cluster the satellite image exporting preliminary classification [52–54]. Merging or reclustering and remapping the cluster numbers resulted in the 7 final land use maps. The classification was carried out using the Google Earth Engine platform [54].

Table 1. Bands and Landsat images used for the years analyzed.

	1985	1990	1995	2000	2005	2010	2015
Images	Landsat 4 TM/Landsat 5 TM	Landsat 4 TM/Landsat 5 TM	Landsat 5 TM	Landsat 5 TM/Landsat 7 ETM+	Landsat 5 TM	Landsat 5 TM	Landsat 8 OLI
Bands			B1/B2/B3/B4/B5/B7				B2/B3/B4/B5/B6/B7
Horizontal Resolution				30 m			

4.2. State Vector, Transition Matrix, and Visualization

Mapping the spatial layout is traditionally based on a classification of land use. However, visualizing changes in land use remains a challenge. A method that combines the state vectors and transition matrix of land use and the Sankey chart was used in this study to analyze the process of urbanization in Nanjing. The transition matrix is a matrix to describe the changes in quantity from the former state to the latter state with the equations as follows:

$$P^{former} = \begin{bmatrix} P^1 & P^2 & \cdots & P^i & \cdots & P^m \end{bmatrix} \tag{1}$$

where P^i = percentage of the total for land use type *i* at the former time, and $\sum_{i=1}^{m} P^i = 1$;

$$P_{latter} = \begin{bmatrix} P_1 & P_2 & \cdots & P_j & \cdots & P_n \end{bmatrix} \tag{2}$$

where P_j = percentage of the total for land use type *j* at the later time, and $\sum_{j=1}^{n} P_j = 1$;

$$P = \begin{bmatrix} P_1^1 & P_2^1 & \cdots & P_j^1 & \cdots & P_n^1 \\ P_1^2 & P_2^2 & \cdots & P_j^2 & \cdots & P_n^2 \\ \vdots & \vdots & \ddots & \vdots & \ddots & \vdots \\ P_1^i & P_2^i & \cdots & P_j^i & \cdots & P_n^i \\ \vdots & \vdots & \ddots & \vdots & \ddots & \vdots \\ P_1^m & P_2^m & \cdots & P_j^m & \cdots & P_n^m \end{bmatrix} \tag{3}$$

where P_j^i = percentage of the total from land use type *i* to type *j*; P_j^i also represents the percentage for which the land use type has not changed when $i = j$; the elements of the matrix match the following rules: $\sum_{j=1}^{n} P_j^i = P^i$, $\sum_{i=1}^{m} P_j^i = P_j$, $\sum_{i=1}^{m} \sum_{j=1}^{n} P_j^i = 1$. The proportion of the part whose land use type has not changed can be calculated by the equation $P_{unchanged} = \sum_{i=1}^{m} P_i^i$. Although it can have different numbers of classes for the different time points, it is recommended to keep them the same, i.e., $m = n$. In addition, the area of the specified land use type can be calculated by the area of the zone multiplied by P^i or P_j, and the area of change flows can be calculated by the area of the zone multiplied by P_j^i.

The use of a Sankey chart to depict the state and dynamic process has been demonstrated in existing studies [55–57]. The original Sankey chart is good at visualizing the

flows and relative visual proportions of components. Its disadvantage is that it has no axis, and thus the value or proportion cannot be read without the help of auxiliary text or annotations. In this paper, an improved method is presented, which combines the Sankey chart and a column chart to make it readable for both states and change flows. The modifications include the following: (1) a Cartesian coordinate plane is placed into the common Sankey chart where the *x*-axis represents time and the *y*-axis the relative contributions of the land use types; (2) for every specific time point, the number of nodes/columns is the number of land use types, and the height of them indicated the percentage of the total for the specific type; (3) the links between two time-verticals represent the transition matrix. This modified Sankey chart depicts the state components at certain time points as well as the change flows of the land use between those in one graph (Figure 3). For the calculation of the status vectors and the transition matrix, we used the Google Earth Engine platform [54], and for the visualizations of the modified Sankey charts, we deployed Observablehq (https://observablehq.com), an interactive JavaScript notebooks platform.

$$P^{former} = \begin{bmatrix} P^1 \\ P^2 \\ \vdots \\ P^i \\ \vdots \\ P^m \end{bmatrix} \qquad P = \begin{bmatrix} P_1^1 & P_2^1 & \cdots & P_j^1 & \cdots & P_n^1 \\ P_1^2 & P_2^2 & \cdots & P_j^2 & \cdots & P_n^2 \\ \vdots & \vdots & \ddots & \vdots & \ddots & \vdots \\ P_1^i & P_2^i & \cdots & P_j^i & \cdots & P_n^i \\ \vdots & \vdots & \ddots & \vdots & \ddots & \vdots \\ P_1^m & P_2^m & \cdots & P_j^m & \cdots & P_n^m \end{bmatrix} \qquad P_{latter} = \begin{bmatrix} P_1 \\ P_2 \\ \vdots \\ P_j \\ \vdots \\ P_n \end{bmatrix}$$
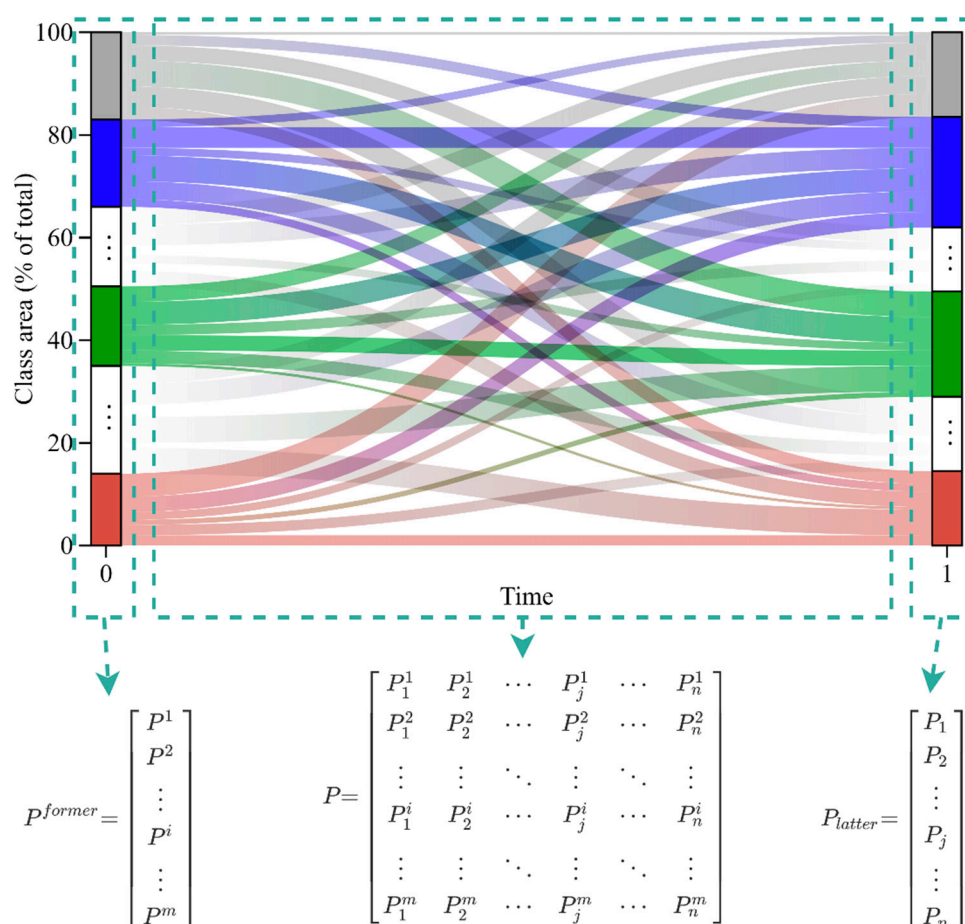
Figure 3. An illustration of the modified Sankey chart. The number of land use types at 0-time and 1-time is assumed to be the same here.

4.3. Precipitation Runoff Volume Control

The definition of volume capture ratio (VCR) is the ratio between the amount captured/retained and the amount of precipitation received at the site over a given period. The sum of VCRa and annual runoff coefficient (RC) equals 1 [58]. The upper limit of short-duration runoff coefficients for different land uses recommended by MOHURD [59] is listed in Table 2.

Table 2. Short-duration runoff coefficient (upper limit) for land use/land cover.

LULC Type	Short-Duration Runoff Coefficient *
Urban and built-up lands	0.8
Mixed forests	0.1
Croplands	0.15
Grasslands	0.1

* Upper limit value sourced from recommendations of short-duration runoff coefficients for stormwater in GB50400-2016 [59].

For an urban zone composed of multiple land use/land cover types, a short-duration composite runoff coefficient can be determined by the area-weighted equation as follows:

$$RC_c = \frac{\sum_{i=1}^{n}(RC_i \cdot A_i)}{\sum_{i=1}^{n} A_i} = \frac{\sum_{i=1}^{n}(RC_i \cdot P_i)}{\sum_{i=1}^{n} P_i} \tag{4}$$

where RC_c represents the short-duration composite area-weighted average runoff coefficient, and RC_i, A_i, and P_i are the short-duration runoff coefficient, area, and percentage of the total area for the land use type i, respectively. Owing to the storage function of water bodies, the land use of water bodies is not considered part of the composed runoff coefficient. Moreover, it is widely recognized that the annual RC is smaller than the event-based short-duration RC due to the consideration of those rainfall events that do not produce any runoff [60]. As an inference, the short-duration RC can be considered as the upper limit of the annual RC, i.e.,

$$RC_{annual}^{upper} = RC_{event} \tag{5}$$

where RC_{annual}^{upper} represents the upper limit of the annual runoff coefficient and RC_{event} is the event-based composite runoff coefficient for each zone.

The lower limit of VCRa ($VCRa - L$) would be reasonable to depict the background value of the VCRa before the implementation of SCC measures, which can be calculated by the following equation:

$$VCRa - L = VCR_{annual}^{lower} = 1 - RC_{annual}^{upper} = 1 - RC_{event} \tag{6}$$

where $VCRa - L$, short for VCR_{annual}^{lower}, refers to the lower limit of the VCRa.

5. Results and Discussion

5.1. LULC Changed from 1985 to 2015 at the City Level

To avoid a massive pile-up of data and graphs, we highlighted three years in the results: 1985, 2000, and 2015 (Figure 4). The states of land use in Z01 (which covers the majority of the urban area in Nanjing) changed considerably (Tables A1–A3, and Figure 5). The urban and built-up areas quadrupled from 11.09% of the total in 1985 to 44.07% in 2015, representing an absolute area size of 139 km² in 1985 to of 554 km² in 2015. The observed changes were mainly due to the rapid growth of the economy and urban population over the past few decades [61,62], a trend that has been seen everywhere in the territory of China. The area of water bodies increased by 20% in 2000 compared to 1985, which may be caused by the misclassification of the northwest shore of the Yangtze River. The water bodies in Z01 are mainly located at the Yangtze River and the Xuanwu Lake, which are protected areas for nature conservation to avoid its disappearance as a result of the rapid process of urbanization. The state values of mixed forests for the three years have not changed much, but the spatial distribution has changed greatly. This indicates that a transformation has occurred from a centralized forest or wood of the outskirt in 1985 to a built-up area with widely distributed greening trees in 2015 (Figure 5). The croplands in Nanjing decreased irreversibly and the loss of its area was about 285 km². The decrease of the croplands contributes to the majority of the increase of the urban and built-up lands. Grasslands made up the least area of land-use in Nanjing and its proportion remained relatively stable,

while the spatial distribution changed considerably over the years. The reason may be that most of the grassland areas in the urban area are cultivated grass patches to serve the local needs of the citizens.
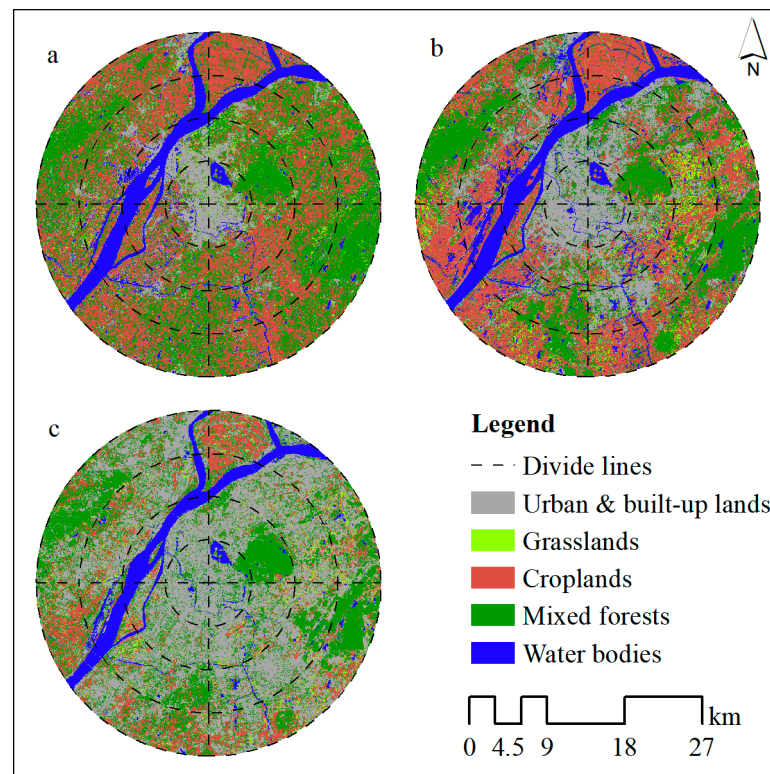

Figure 4. The land use/land cover classification maps covering the majority of the urban area in Nanjing in (**a**) 1985, (**b**) 2000, and (**c**) 2015.
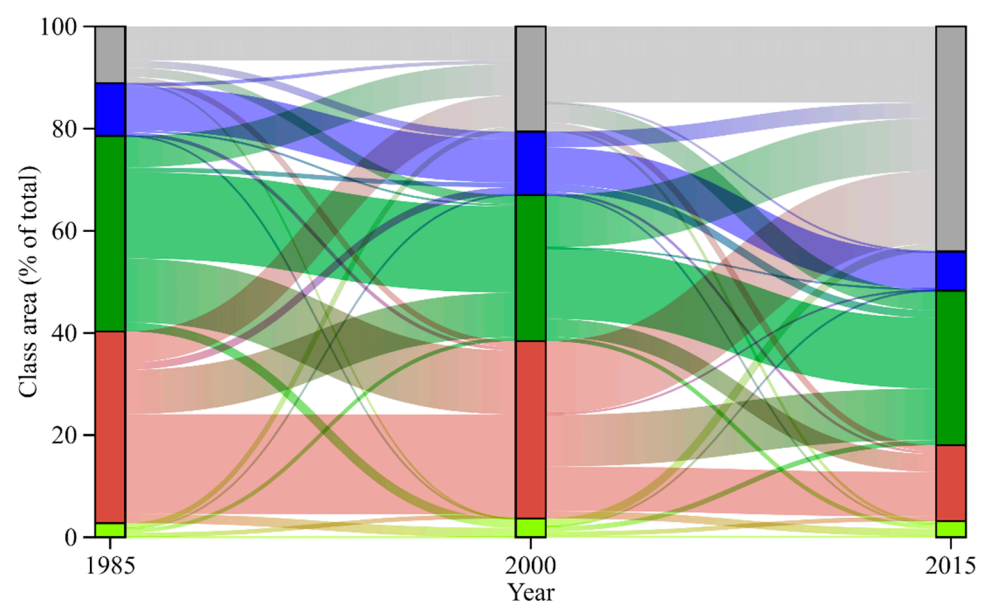

Figure 5. The modified Sankey chart to visualize the state and change flows of the land use and land cover (LULC) classification for Z01 from 1985 to 2015 in Nanjing (colors and classes of the Sankey charts produced in this study are the same as in Figure 4).

To distinguish the different LULC changes from the central district to the outskirts of Nanjing, we investigated the LULC changes of the concentric zones from Z02 to Z05

and the concentric pie zones from Z06 to Z21. The graphs of these results are shown in Figures A1 and A2.

5.2. VCRα-L

$VCRa - L$, the lower limit of the VCRa, was designed as a baseline indicator to evaluate the pre-development stage of an SCC project. Figure 6 shows the spatial distribution of $VCRa - L$ on the city-level from 1985 to 2015. Overall, 89% of the land area had a high $VCRa - L$ of over 0.8 in 1985, and this proportion dropped to 54% in 2015. The numbers illustrate that more than half the area still meets the target of SCC in Z01. Nevertheless, the results of the composite $VCRa - L$ for concentric pie zones showed a great difference. Overall, the value of $VCRa - L$ increased with the distance away from the urban center. The smallest value always appeared at Z02 and the largest value always occurred at Z05 for these three time slices. On the other hand, $VCRa - L$ decreased from 1985 to 2015. The values of $VCRa - L$ in half of the zones were greater than 0.8 in 1985, and there were only three zones with a value below 0.5, which were Z06, Z14, and Z18. In 2000, two zones had an $VCRa - L$ greater than 0.8; however, in 2015, none of them exceeded 0.8, and the eight zones were all less than 0.5. This indicates no subzone meeting the SCC target. The achievability varied for different subzones, i.e., Z18 is the most challenging subzone while Z21 is the easiest one, without consideration of the land area. High-density built-up in the center of Nanjing would be a tough project for SCC.
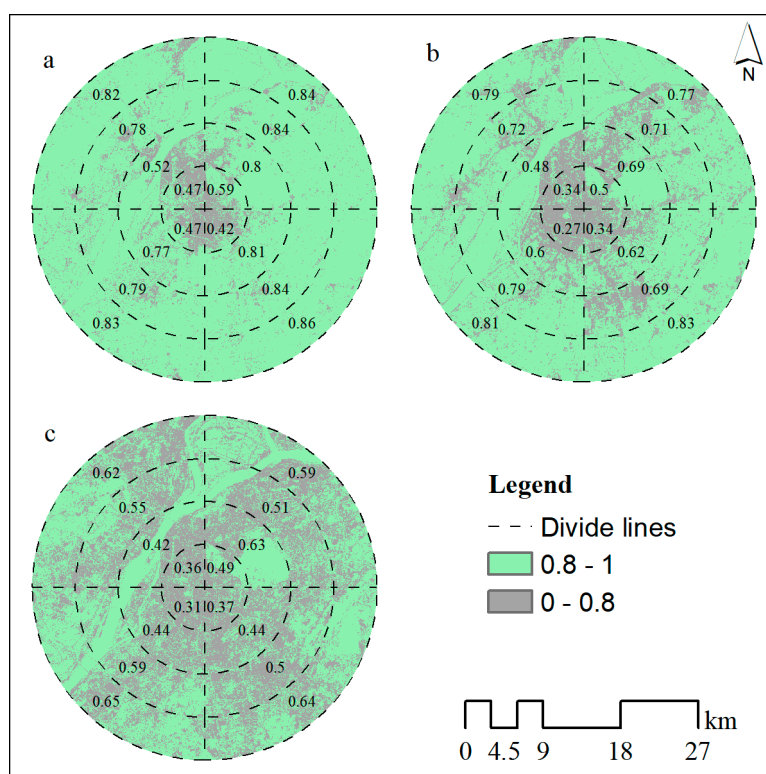

Figure 6. The spatial distribution of *VCRα-L* on the city-level of Nanjing in (**a**) 1985, (**b**) 2000, and (**c**) 2015. The composite *VCRα-L* for the concentric pie zones was annotated by text.

6. Conclusions

VCRa is a key performance indicator for the design and evaluation of SCC measures, but its assessment remains a challenge, particularly at the city level. A set of innovative methods using LULC data derived from remotely sensed Landsat images was developed and demonstrated in this research to conduct a baseline assessment (pre-development stage) of VCRa. For this purpose, a modified Sankey chart to visualize the states and change flows of LULC was developed. This method unifies mathematical descriptions

and visualization of the state vectors and transition matrix to reveal the percentages and pathways of LULC changes. This novel and practical partitioning method has three advantages for its application in built-up regions: (i) it circumvents the variability of urban administrative boundaries, (ii) it enables a comparison between cities and districts within a city, and (iii) it allows for a comparison of LULC between different historical time periods for cities with rapid growth. Moreover, a new ready-to-use indicator, $VCRa - L$, was proposed to evaluate the hydrological characteristics in the pre-development stage of built-up areas of a city and thus to set a baseline for the planning, design, and implementation of SCC projects.

A case study was conducted using the main built-up area of Nanjing (Z01) in China. These Sankey charts revealed the various LULC change pathways of urban landscape as follows: (i) significant changes of LULC occurred in Nanjing from 1985 to 2015, resulting from a rapid expansion of the built-up areas, a decrease of the croplands, and relatively limited changes of the surface areas of water bodies and green space; (ii) the built-up areas remained stable in the centrum zone (Z02), while the surface area of green space increased and of cropland almost disappeared, with the surface area of cropland decreasing significantly but still remaining important in the outskirt zone (Z05); (iii) preferential expansion of built-up areas occurred in the direction of southeast–northwest. From the perspective of $VCRa - L$, in 2015, more than half of the total city surface area still met the target of SCC, but none matched the target of 80% in the subzones.

The above case study further demonstrates that the modified Sankey chart method discloses LULC change pathways and patterns, which provide valuable historical information to understand the underlying causes of hydrological regime shifts required to identify realistic and effective SCC measures. The indicator $VCRa - L$ can help policymakers and city planners to prioritize and select regions to implement SCC measures, to set realistic SCC targets, and to prioritize SCC projects. A shortcoming of the proposed method is that it does not allow an assessment at the level of a SCC project since its physical boundaries are set by functional or legal requirements instead of an arbitrarily chosen grid size.

Author Contributions: Conceptualization, X.L. and C.Z.; methodology, X.L.; software, X.L.; validation, X.L.; formal analysis, X.L.; investigation, X.L.; resources, X.L.; data curation, X.L.; writing—original draft preparation, X.L.; writing—review and editing, C.Z., T.B., and M.Y.; visualization, X.L.; supervision, D.F. and C.Z.; project administration, D.F. and C.Z.; funding acquisition, X.L., D.F., and M.Y. All authors have read and agreed to the published version of the manuscript.

Data Availability Statement: The high-resolution LULC images for Nanjing at five-yearly intervals from 1985 to 2015 have been archived on Google Earth Engine Asset and Zenodo [63]. Moreover, the original data of the state vectors and transition matrixes of the LULC classification in Nanjing used to create the modified Sankey charts have been shared on Zenodo as well [64]. It would be easy to reuse for further analysis and will be distributed to those interested.

Conflicts of Interest: The authors declare no conflict of interest.
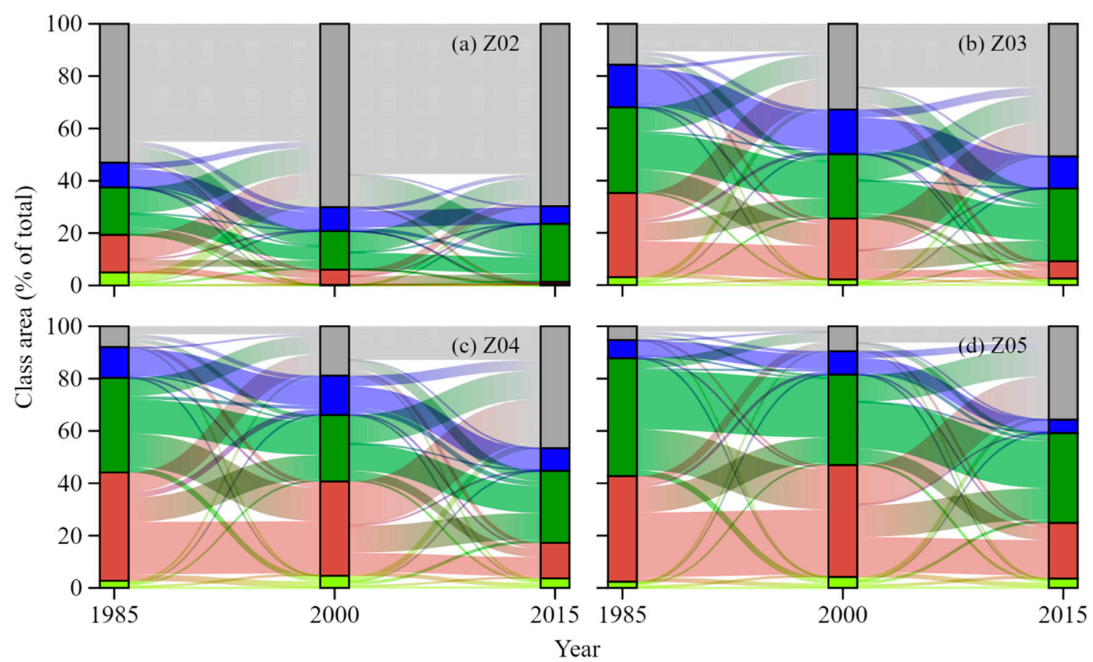
Appendix A

Figure A1. The modified Sankey charts to visualize the state and change flows of LULC for concentric zones (Z02–Z05) in Nanjing from 1985 to 2015.
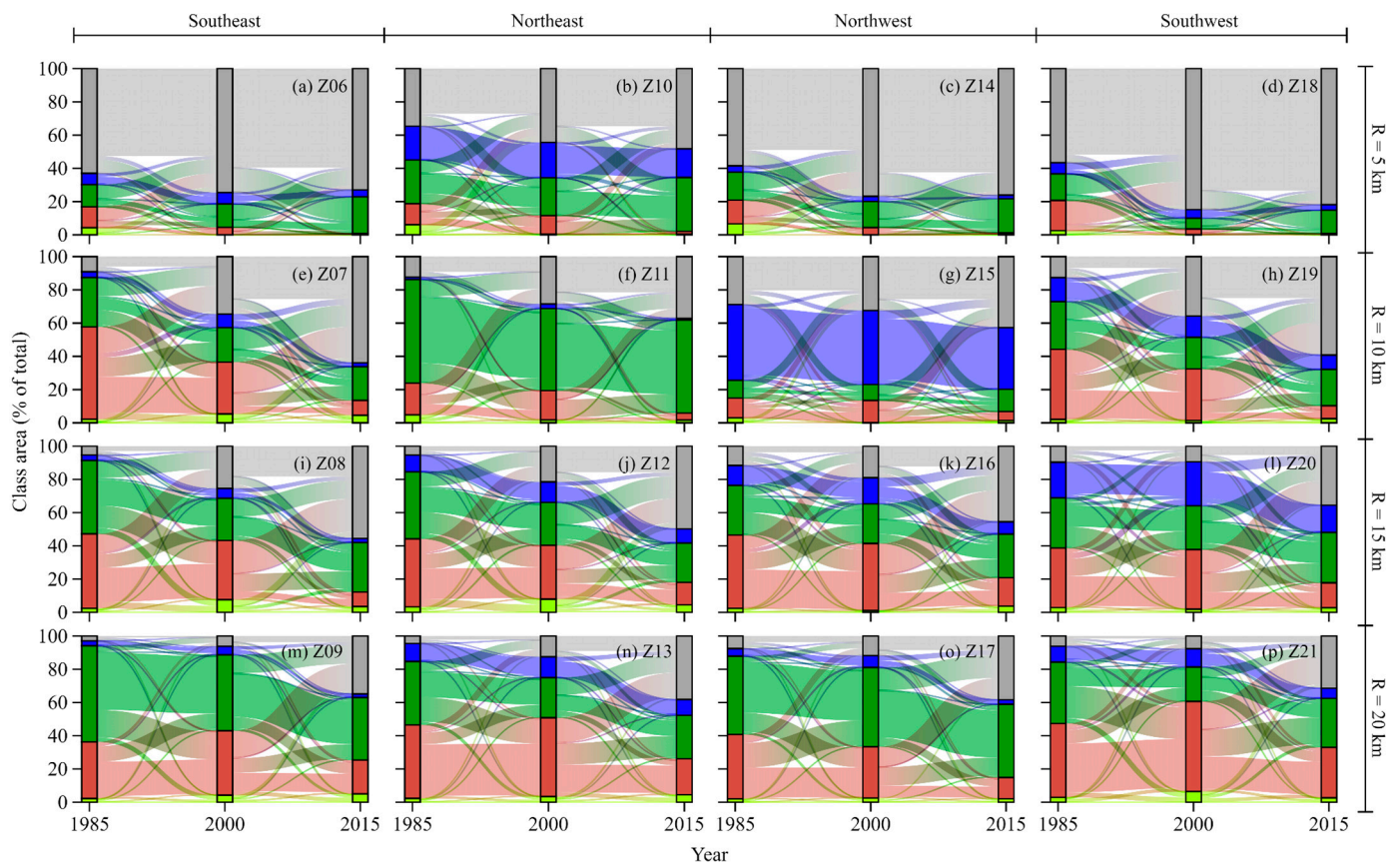

Figure A2. The modified Sankey charts to visualize the state and change flows of LULC for concentric pie zones (Z06–Z21) in Nanjing from 1985 to 2015.

Table A1. The state vectors of land use/land cover classification for Z01 in 1985, 2000, and 2015 (%).

Year	Urban and Built-Up Lands	Water Bodies	Mixed Forests	Croplands	Grasslands
1985	11.09	10.35	38.26	37.54	2.76
2000	20.6	12.41	28.58	34.74	3.67
2015	44.08	7.66	30.23	14.85	3.18

Table A2. The transition matrix of land use/land cover classification for Z01 from 1985 to 2000 (%).

	Urban and Built-Up Lands	Water Bodies	Mixed Forests	Croplands	Grasslands
Urban and built-up lands	6.64	1.44	1.81	1.14	0.06
Water bodies	0.7	8.52	0.41	0.71	0
Mixed forests	6.17	0.91	16.91	12.51	1.77
Croplands	6.09	1.43	8.69	19.52	1.82
Grasslands	1	0.1	0.77	0.86	0.02

Table A3. The transition matrix of land use/land cover classification for Z01 from 2000 to 2015 (%).

	Urban and Built-Up Lands	Water Bodies	Mixed Forests	Croplands	Grasslands
Urban and built-up lands	14.91	0.09	3.83	1.22	0.55
Water bodies	3.09	7.21	1.49	0.51	0.1
Mixed forests	10.29	0.1	13.83	3.53	0.83
Croplands	14.21	0.25	10.1	8.71	1.47
Grasslands	1.57	0.01	0.98	0.89	0.23

References

1. Han, F.; Xu, J.; He, Y.; Dang, H.; Yang, X.; Meng, F. Vertical structure of foggy haze over the beijing-tianjin-hebei area in january 2013. *Atmos. Environ.* **2016**, *139*, 192–204. [CrossRef]
2. Li, X.; Gao, Z.; Li, Y.; Gao, C.Y.; Ren, J.; Zhang, X. Meteorological conditions for severe foggy haze episodes over North China in 2016–2017 winter. *Atmos. Environ.* **2019**, *199*, 284–298. [CrossRef]
3. Fan, L.; Sha, H.; Pang, Y. Water environmental capacity of lake Taihu. *J. Lake Sci.* **2012**, *24*, 693–697. [CrossRef]
4. Zhang, C.; Xie, G.; Lu, C. Research on scarcity degree of chinese water environment capacity and its interactions with regional function. *Resour. Sci.* **2009**, *31*, 559–565.
5. Wang, X.; Wang, Y.; Sun, C.; Pan, T. Formation mechanism and assessment method for urban black and odorous water body: A review. *Chin. J. Appl. Ecol.* **2016**, *27*, 1331–1340. [CrossRef]
6. Yang, Z.; Zhang, M.; Shi, X.; Kong, F.; Ma, R.; Yu, Y. Nutrient reduction magnifies the impact of extreme weather on cyanobacterial bloom formation in large shallow Lake Taihu (China). *Water Res.* **2016**, *103*, 302–310. [CrossRef] [PubMed]
7. Schueler, T.R. The importance of imperviousness. *Watershed Prot. Tech.* **1995**, *1*, 100–111.
8. Federal Interagency Stream Restoration Working Group (FISRWG). *Stream Corridor Restoration: Principles, Processes, and Practices.*; Federal Interagency Stream Restoration Working Group (FISRWG): Washington, DC, USA, 1998; ISBN 0-934213-59-3.
9. Yu, M.; Li, Q.; Hayes, M.J.; Svoboda, M.D.; Heim, R.R. Are droughts becoming more frequent or severe in china based on the standardized precipitation evapotranspiration index: 1951–2010? *Int. J. Climatol.* **2014**. [CrossRef]
10. Edogawa River Office Metropolitan Outer Area Underground Discharge Channel. Available online: https://www.ktr.mlit.go.jp/edogawa/edogawa_index045.html (accessed on 3 October 2019).
11. Beijing Municipal Administration of Quality and Technology Supervision. *Code for Design of Stormwater Management and Harvest Engineering (DB11/685-2013)*; Beijing Municipal Administration of Quality and Technology Supervision: Beijing, China, 2013.
12. National Research Council. *Urban Stormwater Management in the United States*; National Research Council: Washington, DC, USA, 2008; ISBN 0-309-12540-5.
13. Clar, M.L.; Barfield, B.J.; O'Connor, T.P. *Stormwater Best Management Practice Design Guide Volume 1—General Considerations*; U.S. Environmental Protection Agency: Washington, DC, USA, 2004; p. 179.
14. Victoria State Government; Melbourne Water. *Water Sensitive Urban Design Guidelines—South Eastern Councils*; Melbourne Water: Melbourne, VIC, Australia, 2013; p. 44.

15. Andoh, R.Y.G.; Iwugo, K.O. Sustainable urban drainage systems: A UK perspective. *Glob. Solut. Urban Drain.* **2002**, 1–16. [CrossRef]

16. Kondratenko, J.; Ievina, D.; Kuusemets, V.; Mandre, G.; Balicka, J.; Grivina, I.; Ruksane, I.; Tamm, O.; Grants, P. *Handbook on Sustainable Urban Drainage Systems*; Drain for Life: Tartu, Estonia, 2014; p. 121.

17. Lashford, C.; Rubinato, M.; Cai, Y.; Hou, J.; Abolfathi, S.; Coupe, S.; Charlesworth, S.; Tait, S. SuDS & Sponge Cities: A Comparative analysis of the implementation of pluvial flood management in the UK and China. *Sustainability* **2019**, *11*, 213. [CrossRef]

18. *Public Utilities Board (PUB) Active, Beautiful, Clean Waters Design Guidelines*, 4th ed.; Public Utilities Board: Singapore, 2018; p. 112.

19. Cui, G.; Zhang, Q.; Zhan, Z.; Chen, Y. Research progress and discussion of sponge city construction. *Water Resour. Prot.* **2016**, *32*, 1–4. [CrossRef]

20. Ministry of Housing and Urban-Rural Development (MOHURD). *Technical Guide for Sponge City Construction—Low Impact Development Stormwater Management System*; Ministry of Housing and Urban-Rural Development (MOHURD): Beijing, China, 2014.

21. Zhang, K.; Che, W.; Zhang, W.; Zhao, Y. Discussion about initial runoff and volume capture ratio of annual rainfall. *Water Sci. Technol.* **2016**, *74*, 1764–1772. [CrossRef] [PubMed]

22. Randall, M.; Sun, F.; Zhang, Y.; Jensen, M.B. Evaluating sponge city volume capture ratio at the catchment scale using SWMM. *J. Environ. Manag.* **2019**, *246*, 745–757. [CrossRef]

23. Shamseldin, A.Y. *Review of TP-10 Water Quality Volume Estimation*; Auckland Regional Council: Auckland, New Zealand, 2010; p. 38.

24. United States Environmental Protection Agency (USEPA). *Technical Guidance on Implementing the Stormwater Runoff Requirements for Federal Projects under Section 438 of the Energy Independence and Security Act*; United States Environmental Protection Agency (USEPA): Washington, DC, USA, 2009; p. 63.

25. Stormwater Manager's Resource Center (SMRC) Options for Water Quality Volumes. Available online: https://www.stormwatercenter.net/Manual_Builder/Sizing_Criteria/Water%20quality/Options%20for%20Water%20Quality%20Volumes.htm (accessed on 1 July 2020).

26. Beech, A.; Earthfx. *Runoff Volume Control Targets for Ontario*; Aquafar Beech: Quelph, ON, Canada, 2016; p. 125.

27. Upper Darby Township. *Upper Darby Township Stormwater Management*; Upper Darby Township: Delaware Country, PA, USA, 2005; p. 116.

28. Tang, N.; Che, W. Analysis of the urban stormwater treatment facilities sizing. *Water Wastewater Eng.* **2009**, *35*, 43–48. [CrossRef]

29. Li, J.; Wang, W.; Che, W.; Liu, C.; Zhao, Y. Explanation of Sponge City development technical guide: Regional division for total rainfall runoff volume capture target. *China Water Wastewater* **2015**, *31*, 6–12.

30. Che, W.; Zhao, Y.; Li, J.; Wang, W.; Wang, J.; Wang, S.; Gong, Y. Explanation of Sponge City development technical guide: Basic Concepts and comprehensive goals. *China Water Wastewater* **2015**, *31*, 1–5. [CrossRef]

31. Liu, C.; Zhang, Y.; Wang, Z.; Wang, Y.; Bai, P. The LID pattern for maintaining virtuous water cycle in urbanized area: A preliminary study of planning and techniques for Sponge City. *J. Nat. Resour.* **2016**, *31*, 719–731. [CrossRef]

32. Wang, W.; Li, J.; Che, W.; Zhao, Y. Explanation of Sponge City development technical guide: Planning index for urban total runoff volume capture. *China Water Wastewater* **2015**, *31*, 18–23. [CrossRef]

33. Hunt, W.F.; Lord, W.G. *Bioretention Performance, Design, Construction, and Maintenance*; Urban Waterways: Raleigh, NC, USA, 2004.

34. Hunt, W.F.; Lord, B. *Maintenance of Stormwater Wetlands and Wet Ponds*; Urban Waterways: Raleigh, NC, USA, 2006; pp. 1–10.

35. Hunt, W.F.; Davis, A.P.; Traver, R.G. Meeting hydrologic and water quality goals through targeted bioretention design. *J. Environ. Eng. (United States)* **2012**, *138*, 698–707. [CrossRef]

36. Cizek, A.R.; Hunt, W.F. Defining predevelopment hydrology to mimic predevelopment water quality in stormwater control measures (SCMs). *Ecol. Eng.* **2013**, *57*, 40–45. [CrossRef]

37. Braga, A.; O'Grady, H.; Dabak, T.; Lane, C. Performance of two advanced rainwater harvesting systems in Washington DC. *Water* **2018**, *10*, 667. [CrossRef]

38. Drake, J.A.P. Performance and Operation of Partial Infiltration Permeable Pavement Systems in the Ontario Climate. Ph.D. Thesis, University of Guelph, Quelph, ON, Canada, 2013.

39. Drake, J.; Bradford, A.; Van Seters, T. Stormwater quality of spring-summer-fall effluent from three partial-infiltration permeable pavement systems and conventional asphalt pavement. *J. Environ. Manag.* **2014**, *139*, 69–79. [CrossRef]

40. Jiangsu Provincial Department of Housing and Urban-Rural Development (JPDOHURD). *Jiangsu Province Sponge City Technical rules*; Jiangsu Provincial Department of Housing and Urban-Rural Development (JPDOHURD): Nanjing, China, 2017.

41. General Office of Nanjing Municipal People's Government. *Implementation Opinions on Promoting the Sponge City Construction*; General Office of Nanjing Municipal People's Government: Nanjing, China, 2016; p. 12.

42. Nanjing Sponge City Construction Leading Group Office. *Nanjing City Sponge City Construction Guidelines*; Nanjing Sponge City Construction Leading Group Office: Nanjing, China, 2018.

43. Li, Q.; Wang, F.; Yu, Y.; Huang, Z.; Li, M.; Guan, Y. Comprehensive performance evaluation of LID practices for the Sponge City construction: A case study in Guangxi, China. *J. Environ. Manag.* **2019**, *231*, 10–20. [CrossRef] [PubMed]

44. Ewaters. *Specific Design of Lianyungang Shijifenghuang Community Under the Concept of Sponge City Construction*; Ewaters: Shanghai, China, 2018.

45. RIONED. *Climate Change, Heavier Rainstorms and the Urban Drainage System 2009*; RIONED: Ede, The Netherlands, 2009.

46. Nanjing Statistical Bureau. *Statistical Yearbook of Nanjing: 2019*; China Statistical Press: Beijing, China, 2019.

47. Google Earth Pro V7.3.3.7786 Nanjing City, Jiangsu Province, China. 118°46′43.94″N, 32°02′37.71″E, Eye Alt 190.43 Km. Landsat /Copernicus. 2020. Available online: https://www.earth.google.com (accessed on 20 October 2020).

48. Wang, X.; Xu, G. Adjustments of administrative division in Nanjing. *Xinhua Daily* **2018**, *1*. Available online: http://xh.xhby.net/mp3/pc/c/201808/-17/c520770.html (accessed on 25 September 2019).

49. Google Earth Pro V7.3.3.7786 Nanjing City, Jiangsu Province, China. 118°46′43.94″N, 32°02′37.71″E, Eye Alt 59.97 Km. Maxar Technologies 2020, CNES/Airbus 2020. 2020. Available online: https://www.earth.google.com (accessed on 31 January 2021).

50. Potapov, P.; Hansen, M.C.; Kommareddy, I.; Kommareddy, A.; Turubanova, S.; Pickens, A.; Adusei, B.; Tyukavina, A.; Ying, Q. Landsat analysis ready data for global land cover and land cover change mapping. *Remote Sens.* **2020**, *12*, 426. [CrossRef]

51. Abdi, A.M. Land cover and land use classification performance of machine learning algorithms in a boreal landscape using sentinel-2 data. *GISci. Remote Sens.* **2020**, *57*, 1–20. [CrossRef]

52. Viana, C.M.; Girão, I.; Rocha, J. Long-term satellite image time-series for land use/land cover change detection using refined open source data in a rural region. *Remote Sens.* **2019**, *11*, 1104. [CrossRef]

53. Vali, A.; Comai, S.; Matteucci, M. Deep learning for land use and land cover classification based on hyperspectral and multispectral earth observation data: A review. *Remote Sens.* **2020**, *12*, 2495. [CrossRef]

54. Gorelick, N.; Hancher, M.; Dixon, M.; Ilyushchenko, S.; Thau, D.; Moore, R. Google Earth engine: Planetary-scale geospatial analysis for everyone. *Remote. Sens. Environ.* **2017**, *202*, 18–27. [CrossRef]

55. Cuba, N. Research note: Sankey diagrams for visualizing land cover dynamics. *Landsc. Urban Plan.* **2015**, 5. [CrossRef]

56. Li, Y.; Li, Y.; Fan, P.; Sun, J.; Liu, Y. Land use and landscape change driven by gully land consolidation project: A case study of a typical watershed in the loess plateau. *J. Geogr. Sci.* **2019**, *29*, 719–729. [CrossRef]

57. Da Silva, R.F.B.; Millington, J.D.A.; Moran, E.F.; Batistella, M.; Liu, J. Three decades of land-use and land-cover change in mountain regions of the Brazilian Atlantic forest. *Landsc. Urban Plan.* **2020**, *204*, 103948. [CrossRef]

58. Ministry of Housing and Urban-Rural Development (MOHURD). *Assessment Standard for Sponge City Effects (GB/T51345-2018)*; China Construction Industry Press: Beijing, China, 2018.

59. Ministry of Housing and Urban-Rural Development (MOHURD). *Technical Code for Rainwater Management and Utilization of Building and Sub-District (GB50400-2016)*; China Construction Industry Press: Beijing, China, 2016.

60. Critchley, W.; Siegert, K. *Water Harvesting*; Food and Agriculture Organization of the United Nations (FAO): Rome, Italy, 1991.

61. Shi, G.; Ye, P.; Ding, L.; Quinones, A.; Li, Y.; Jiang, N. Spatio-temporal patterns of land use and cover change from 1990 to 2010: A case study of Jiangsu Province, China. *Int. J. Environ. Res. Public Health* **2019**, *16*, 907. [CrossRef] [PubMed]

62. Du, X.; Jin, X.; Yang, X.; Yang, X.; Zhou, Y. Spatial pattern of land use change and its driving force in Jiangsu Province. *Int. J. Environ. Res. Public Health* **2014**, *11*, 3215–3232. [CrossRef]

63. Liu, X. High-resolution (30m) LULC images for Nanjing. *Zenodo* **2019**. [CrossRef]

64. Liu, X. The state vectors and transition matrixes of the LULC classification in Nanjing for modified Sankey chart. *Zenodo* **2019**. [CrossRef]